Thermo-mechanical modelling of laser welding process on aluminium alloy EN AW 6082-T6

ER Imam Fauzi¹ · Z Samad¹ · NM Nor¹ · MSC Jamil² · AM Najib³

Received: XX Feb 2019 / Accepted: YY July 2019

© The Author(s) 2019

Abstract

In present work, finite element method (FEM) is implemented to investigate the temperature distribution in laser welding of 5mm thick aluminium alloy EN AW 6082-T6. The Gaussian heat source model was used to analyse the influence of peak temperature to the radial distance from the center of the heat source and the thickness of the plate. Temperature-dependent thermal properties of aluminium alloy and the convective-radiative boundary conditions were included in the model. The finite element code, ANSYS along with APDL command subroutines was employed to obtain the numerical results. The effect of heat input and welding speed on the weld pool shape and temperature distribution were investigated. Finally, the predicted temperature distribution and the size of heat-affected zone were compared with the experimental results. The comparison shows that they are in good agreement.

Keywords Laser welding · Modelling · Finite element · Aluminium alloy

1 Introduction

Without doubt, the continued development of aluminium can be primarily attributed to this material's many desirable physical characteristics, which are comparatively light weight, high strength, versatility of both extruding and casting, and excellent corrosion resistant. In conjunction with the continually developing environmental issues, the superior recycling capability of aluminium makes it an excellent choice for a wide variety of applications. With increasing demand of aluminium in engineering field, the development of aluminium welding technology is undeniably evolved to improve the structural integrity of aluminum alloys itself. However, one of the most severe challenges in aluminium welding is the occurrence of heat-affected-zone (HAZ), which may results in a significantly reduced strength compared to the base metal. This phenomenon, which also known as softening, is significant factor in the heat-treatable alloys particularly in 6000 and 7000 series, and in 5000 series alloys in a workhardened temper condition. In case of the 6000 series alloys, the heat dissipation during welding can locally reduce the parent metal strength on the order of 30%-50% and the HAZ normally extends between 10mm-30mm from the centre of the weld [1-3]. However, according to Eurocode 9 [4], the extent of this zone depends on the welding method, element thickness, alloying elements and temper designation, while the severity is largely a function of the parent metal used.

[■] ER Imam Fauzi elfirahayu2006@yahoo.com

¹Manufacturing Engineering Group, School of Mechanical Engineering, Universiti Sains Malaysia (USM), 14300 Nibong Tebal, Penang, Malaysia

²Dscaff Group, Mount Kiara, Kuala Lumpur, Malaysia

³Fakulti Kejuruteraan Pembuatan, Universiti Teknikal Malaysia Melaka (UTeM), Hang Tuah Jaya 76100 Durian Tunggal, Melaka, Malaysia.

Interest in laser welding applications has continued to increase due to its advantage of precision joining. In understanding the physical behavior during laser welding process, careful observations and investigations have been carried out numerously. Experimental based evaluations to evaluate the mechanical properties and microstructural effects of laser welded components [5–9] currently provide insufficient insight into critical aspects of molten pool formation and physic of the process itself. Therefore, numerical simulations of laser welding process have long been employed to analyze and predict the deformation, molten behavior, thermal, fluid, and residual stress effects on the laser welded components [10–14]. Additionally, the issue of softening behaviour of aluminium laser welded joint also became an interest amongst researchers. Attempts to predict the HAZ characteristic of laser welded component were carried out experimentally and numerically in [15–18]. Although the used of computational analysis to compute the HAZ dimension was widely adapted today, a necessity of accurate material properties and detailed meshes may lead to design difficulties. Therefore, a simple model with more general material properties is needed for HAZ prediction. In this study, a numerical model to predict temperature distribution and the width of heat-affectedzone was proposed. The obtained numerical results were in good agreement with experimental data. It can be used in practical simulations of laser welded aluminium alloy connections to reduce a need of extensive mechanical testing, particularly in mapping the width of HAZ.

2 Experimental Procedure

Laser aluminium welding was conducted with the collaboration of Singapore Manufacturing Technology (SIMTech) laboratory. A 6kW laser welding system was used for these experiments, as shown in Figure 1. Laser power and welding speed were varied in five (5) levels; laser power (2.5kW to 4.5kW) and welding speed (0.9 m/min to 1.5 m/min). The operation range of the laser welding experiment was determined based on a preliminary test run by SIMTech.

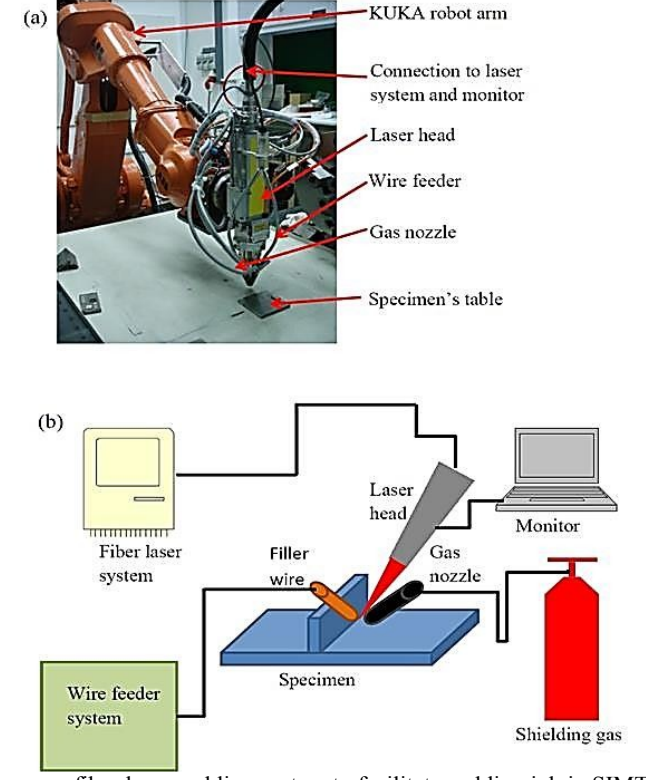


Fig. 1 (a) 6kW high power fiber laser welding system to facilitate welding job in SIMTech, Singapore [19] (b)

Schematic diagram of laser welding process

The material used in this study is aluminium alloy EN AW 6082 in T6 condition. The welding coupons were cut by an abrasive water-jet cutting system with the dimensions of 120 mm x 120 mm x 5 mm and 120 mm x 60 mm x 3mm. The 5 mm-thickness plate was selected to be the base material, whereas the 3 mm-thickness plate was used as the flange material with designed bevel of 45° to ensure full penetration of the weld seam. The flange material was tightly clamped, 90° from the base material and a zero gap was assumed to be achieved.

3 Numerical Model of Thermal Analysis

3.1 Material Model

In order to accurately capture the occurring phenomena during the thermal cycle, the graded-mesh construction was used for the analysis. This approach is based on a dense mesh division along the weld line and its adjacent zone. The mesh size became coarser as the distance from the weld bead zone increase. It was constructed primarily of solid hexahedral element SOLID70, except in transition areas of thin to coarse mesh, where the tetrahedral SOLID87 element is required. To reduce the computational time, only half of the actual length and width of the specimen was taken into account throughout the analysis. Figure 2(a) and 2(b) show the considered model of the T-joint profile for the analysis and the mesh density transition for the model respectively.

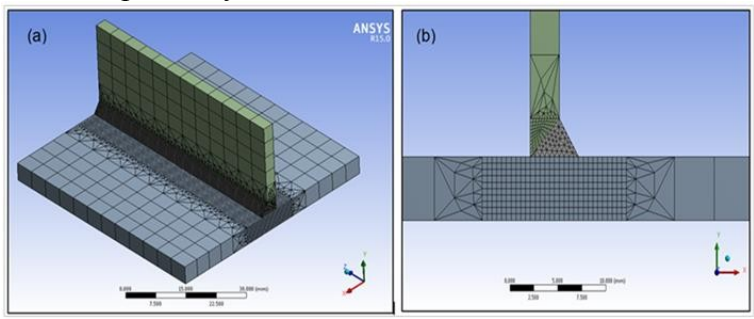


Fig. 2 (a) T-joint profile for thermal model analysis. (b) Mesh density transition of thermal model

A sequence of convergence tests has been conducted to select suitable element size particularly in the thickness direction and at the region near the weld line. Several levels of meshes with varying element numbers from 200,000 to 500,000 in scales of width, length and thickness are chosen to determine the effect of element size on the convergence of computations. The simulated peak temperature becomes independent on the mesh density of 350,000 elements as shown in Figure 3. Therefore, a mesh of over 350,000 elements was employed to the model. Nearby and along the weld bead area, the chosen element size is 0.1 mm, whereas element size of 5 mm is employed in the coarser region. A free mesh was used in order to connect these two regions.

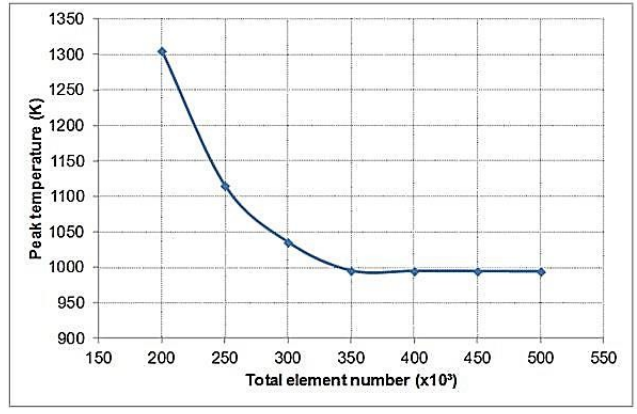


Fig. 3 The mesh convergence parametric study

3.2 Heat Source Model

In this model, the total heat input was solely the arc heat input. Due to involvement of high energy heat sources of laser beam, the necessary heat source model preferred is the Gaussian heat source distribution, as depicted in Figure 4, where the heat flux deposited on the surface of the workpiece [20]. The contour plot of the moving Gaussian heat source model is illustrated in Figure 5, where isotherm lines were evident. The first model of Gaussian distribution was first made by Pavelic et al. [21], which also known as Pavelic's disc, due to the circular form of heat concentration. The improved model, which was computed using Rosenthal's model, achieves significantly better temperature distribution. In this model, the thermal flux can be expressed by the following equation [22]:

$$q(x,z,t) = \frac{3Q}{\pi r_B^2} e^{-3x^2/r_B^2} e^{-3[z+v(\tau-t)]^2/r_B^2}$$
(1)

where Q is the energy input, r_B denotes the characteristic radius of the heat flux distribution, v is the welding speed, and τ is a fictive time factor needed to define the position of the heat source at time t = 0.

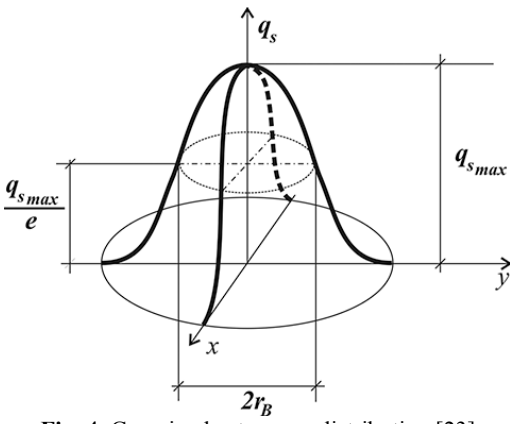


Fig. 4 Gaussian heat source distribution [23]

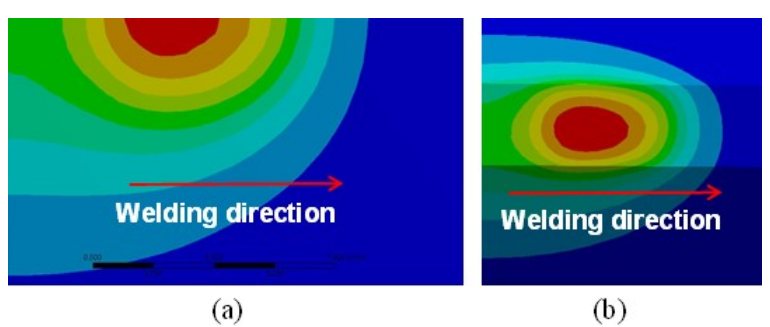


Fig. 5 Gaussian heat source model for thermal analysis from (a) side view and (b) top view

In laser welding simulation, the heat input depends on the supplied laser beam energy and absorption properties of the material surface. In the present study, the moving heat source was modeled as a Gaussian distribution with the intensity of:

$$I_Q(x, y, z) = \frac{\eta P_L}{2\pi\sigma^2} e^{-(r^2/2\sigma^2)}$$
 (2)

where P_L is laser power, η is the efficiency coefficient, and σ is the radial distance. During laser welding process, part of the energy supplied by laser source is lost due to the reflection of specimen's surface. It is worth mentioning that the maximum effective input power of heat source is 70% from the nominal laser power in case of aluminium [24]. Therefore, η is taken to be 0.3.

3.3 Material Properties and Boundary Conditions

By assuming that aluminium alloy EN AW 6082-T6 is homogeneous; the material properties have been selected referencing several material handbooks and journal articles. Available thermo-physic properties of aluminium alloy EN AW 6082-T6 were used to establish standard reference data according to the ambient, melting and boiling points as given in Table 1. The mechanical properties, such as density, Young's modulus, thermal conductivity, specific heat capacity, and the yield stress, which are usually measured in the vicinity of ambient temperature, are assumed to be dependent to the temperature change as presented in Figure 6. Only Poisson's ratio is kept constant throughout the simulation.

Table 1 Available experimental thermo-physical properties of EN AW 6082-T6 [13]

Properties	Symbol	Value
Melting point	T_m	660 °C
Solidus temperature	T_s	545 °C
Boiling Temperature	T_b	2467 °C
Latent heat	H_v	10.9 kJ/g
Specific heat capacity	C_p	897 J/kgK
Density	ρ	2710 g/cm ³
Thermal conductivity	k	235 W/mK
Young's Modulus	E	70 GPa
Poisson's ratio	υ	0.3
Thermal expansion	a_L	24 x 10 ⁻⁶ K ⁻¹
Diffusivity coefficient	κ	$40 \times 10^{-6} \text{ m}^2/\text{s}$

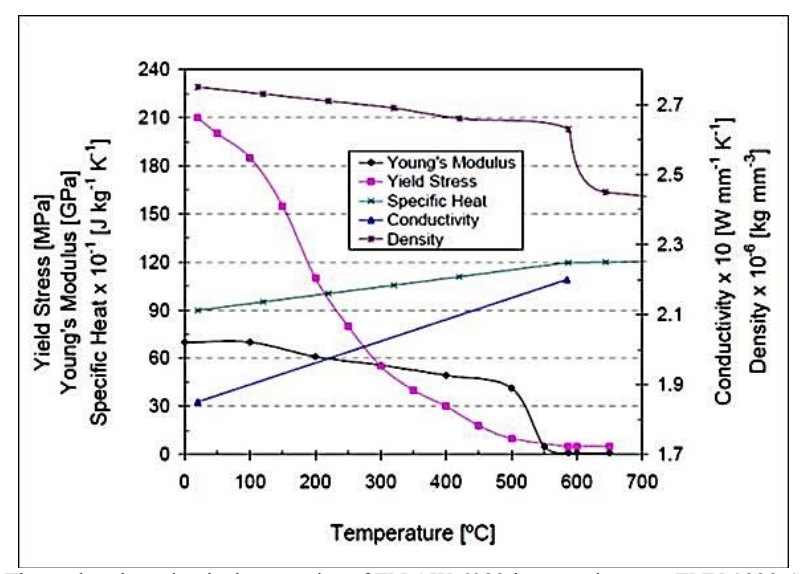


Fig. 6 Thermal and mechanical properties of EN AW 6082 in accordance to ENV 1999-1-2 [25]

The governing differential equation for transient thermal analysis can be expressed as [26]:

$$\rho C_p \frac{\partial T}{\partial \tau} = \frac{\partial}{\partial x} \left(k_x \frac{\partial T}{\partial x} \right) + \frac{\partial}{\partial y} \left(k_y \frac{\partial T}{\partial y} \right) + \frac{\partial}{\partial z} \left(k_z \frac{\partial T}{\partial z} \right) + \dot{q}$$
(3)

where ρ is the density of conducting medium; C_p is the specific heat of the medium; k_x , k_y , k_z are the thermal conductivities of the medium in the x, y, and z direction, respectively; τ is fictive time factor; and \dot{q} is the total heat input. To solve the differential equation, boundary and initial conditions are required. The general form of boundary conditions can be written as:

$$-\left(k_x \frac{\partial T}{\partial x} n_x + k_y \frac{\partial T}{\partial y} n_y + k_z \frac{\partial T}{\partial z} n_z\right) = q_{conv} + q_{rad} - \alpha q_\tau \tag{4}$$

where n_x , n_y , n_z are the direction cosines of the normal to the surface; T_∞ is the ambient temperature; h_{conv} is the convective heat transfer coefficient; α is the absorptivity; and q_τ is the radiant laser heat flux function. The convective heat transfer coefficient was assumed to vary with temperature and defined as:

$$h_{conv} = \frac{kN_u}{L} \tag{5}$$

where k is the thermal conductivity of the material, L is the characteristic length of the surface, and N_u is the Nusselt number:

$$N_u = 5.67 P r^{1/3} G r^{1/3} (6)$$

Here, Pr is the Prandtl number and Gr is the Grashof number. Thermal radiation is assumed from the surface to surroundings. Prior to welding, the material is assumed to be at room temperature. The heat losses due to radiation were modeled by Stefan-Boltzmann relation:

$$q_{rad} = \sigma_{st} \varepsilon_{\tau} (T^4 - T_{\infty}^4) \tag{7}$$

where σ_{st} is Stephan-Boltzmann constant (equal to 5.67 x 10^{-8} W/m²K⁴) and ε_{τ} is the emissivity of the surface ($\varepsilon_{\tau} = 0.05$), in accordance to data published in [27]. The schematic presentation of applied boundary conditions was illustrated in Figure 7.

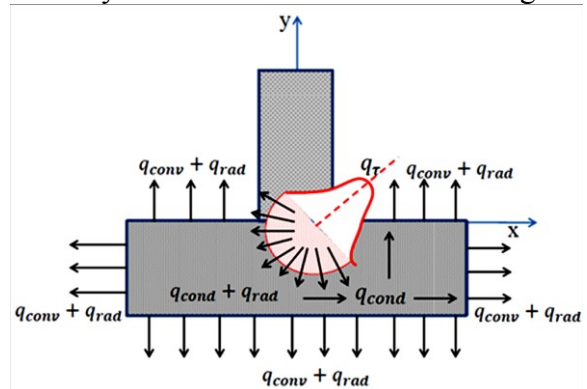


Fig. 7 Schematic presentation of applied boundary conditions for thermal model

3.4 Model Assumption and Validation

The thermal analysis is focused on the prediction of the heat transfer in the weld pool, the temperature distribution in the overall weldment, the size of fusion zone (FZ), heat-affected zone and geometry of the molten pool. The heat-affected zone identification relies upon the experimental data and available data from open literature in [28] and [29], with an assumption that the studied material has an identical chemical composition. It is evident that the reversion of hardening precipitates occurring during the welding process, where the peak temperature range from 220°C to 500°C as depicted in Figure 8(a). However, a large fraction of alloying elements adjacent to the fusion boundary, undergo natural aging after a period of 5-7 days (Figure 8(b)), resulting in a slight increase of hardness values due to the enhancement of hardening precipitates. According to [29] element which experienced a peak temperature of about 220°C and below will recover to its original hardness (base metal) during the natural aging process. According to this model, the HAZ profile was characterized based upon the quasi-stationary temperature distribution around a moving heat source. Therefore, in this study, the HAZ was divided into 2 regions;

- 1) Sub-HAZ 1, where the range of peak temperature, $430^{\circ}\text{C} < T < Solidus temperature}$ (~545°C).
- 2) Sub-HAZ 2, where the range of peak temperature, $220^{\circ}\text{C} < T < 430^{\circ}\text{C}$.

Aside from those regions (where the range of peak temperature, T < 220°C), the material was assume to have the base metal characteristics. The weld pool was considered as the fusion zone (FZ) during

the analysis, by assuming that the material was fully melted at solidus temperature (545°C) and the addition of filler metal will change the Si content in weld zone [30].

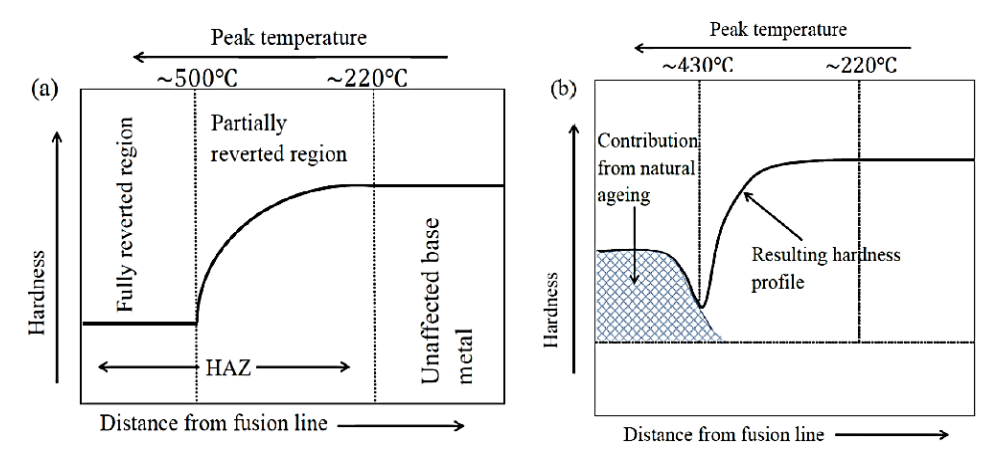


Fig. 8 Schematic diagrams presenting the reactions of precipitates in the HAZ of 6082-T6 weldments: (a) hardness distribution during dissolution process (b) hardness distribution following prolonged natural aging in room temperature [29]

The comparison of the weld pool dimension in Figure 9 verified the correct implementation of the heat source model. In this figure, the picture on the left depicts the obtained weld pool by experiment and the right picture illustrates the computed weld pool in terms of the isotherm contour. The boundary of the molten zone and HAZ in the left pictures was denoted by white lines, whereas the penetration of fusion zone in the right pictures was encompassed by the isotherm line A (liquidus temperature ≈ 545 °C). The boundary of HAZ in the computed figures was indicated by the isotherm line C (lower critical temperature ≈ 220 °C). Therefore, the sub-HAZ 1 and sub-HAZ 2 can be readily determined within isotherm line A and C.

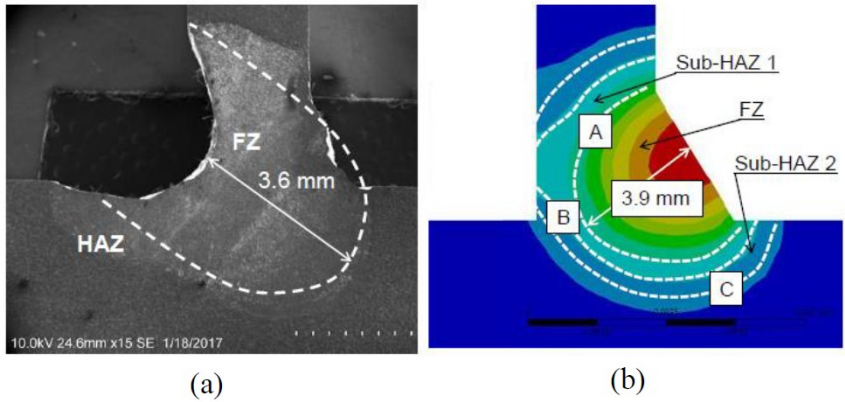


Fig. 9 Weld pool profile obtained by (a) experiment (b) simulation at laser power of 4.5 kW and welding speed of 1.5 m/min

4 Results and Discussions

A set of simulation was conducted to understand the effect of heat input on thermal model. In these cases, the welding velocity remained constant, thus the results presented the effect of heat input variation. Table 2 listed the corresponding simulation data in terms of the weld pool and HAZ dimension. The simulation cases L3 and L5 gave almost similar results with the corresponding experiment data, in which the prediction error of both cases was laid within 0.89% - 5.64%. These results indicate that the thermal model of laser welding was valid for prediction purpose. The case of L3 and ML5 were done for validation purpose because the experimental data were only available for these two cases. Due to the limitation of time and cost, therefore thermal model was used to simulate the other cases (L1, L2 and L4).

Table 2 Simulation and experimental results for heat input variation at constant welding speed of 0.9 m/min

Case	Heat input (kJ/mm)	Depth of FZ (mm)			Width of HAZ (mm)		
		Model	Exp.	% Error	Model	Exp.	% Error
L1	0.15	3.19	-	-	5.12	-	-
L2	0.18	4.47	-	-	6.04	-	-
L3	0.23	4.68	4.43	5.64	6.86	6.80	0.89
L4	0.27	5.04	-	-	7.06	-	-
L5	0.30	5.27	5.21	1.15	6.82	7.20	5.28

Figure 10 illustrates the dependency of penetration depth and width of HAZ on the heat input variation. In general, data fitting resulted in a non-linear relation between the depth of fusion zone and the width of HAZ with the heat input variation. It can be assumed that the penetration depth and the width of HAZ have the tendency to increase with the increase of heat input. However, a slight decrease in the HAZ width was observed for the case of 0.3 kJ/mm heat input. No apparent reason can be offered for this phenomenon. This result may indicate that there is a limit in predicting the HAZ width in the laser welding of thin plates.

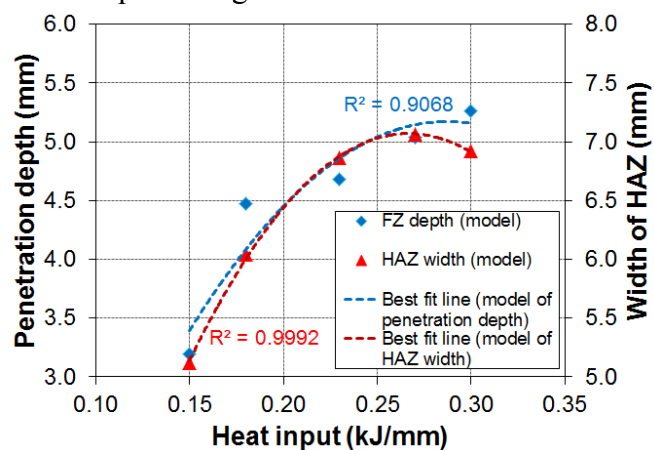


Fig. 10 Plots of penetration depth and width of HAZ against heat input variation with constant welding speed of 0.9 m/min

To understand the effect of welding speed on the thermal model, a set of simulation case has been compared by varying the welding speed and setting a fixed value of laser power at 4.0 kW. Figure 11 presents a comparison of the simulated weld pool shapes made in case L4, L6, L7, L8, and L9. From the results, the depth and the width of the melt pool and HAZ were measured while the welding speed was gradually increased. Table 3 listed the corresponding simulation and some experimental data. From the table, it is evident that the simulation cases L7 and L9 gave almost similar results with the corresponding experimental data. The prediction error of both cases was laid within 2.13% - 4.56%, indicating that the thermal model of laser welding process gives acceptable data prediction for numerical analysis.

Table 3 Simulation and experimental results for welding velocity variation at constant laser power of 4.0 kW

Case	Welding speed (m/min)	Depth of FZ (mm)		Full width of HAZ (mm)			
		Model	Exp.	% Error	Model	Exp.	% Error
L4	0.90	5.04	-	-	7.56	-	-
<i>L6</i>	1.05	4.94	-	-	7.16	-	-
<i>L7</i>	1.20	4.31	4.22	2.13	6.62	6.42	3.12
L8	1.35	3.87	-	-	6.26	-	-
L9	1.50	3.39	3.52	3.69	5.96	5.70	4.56

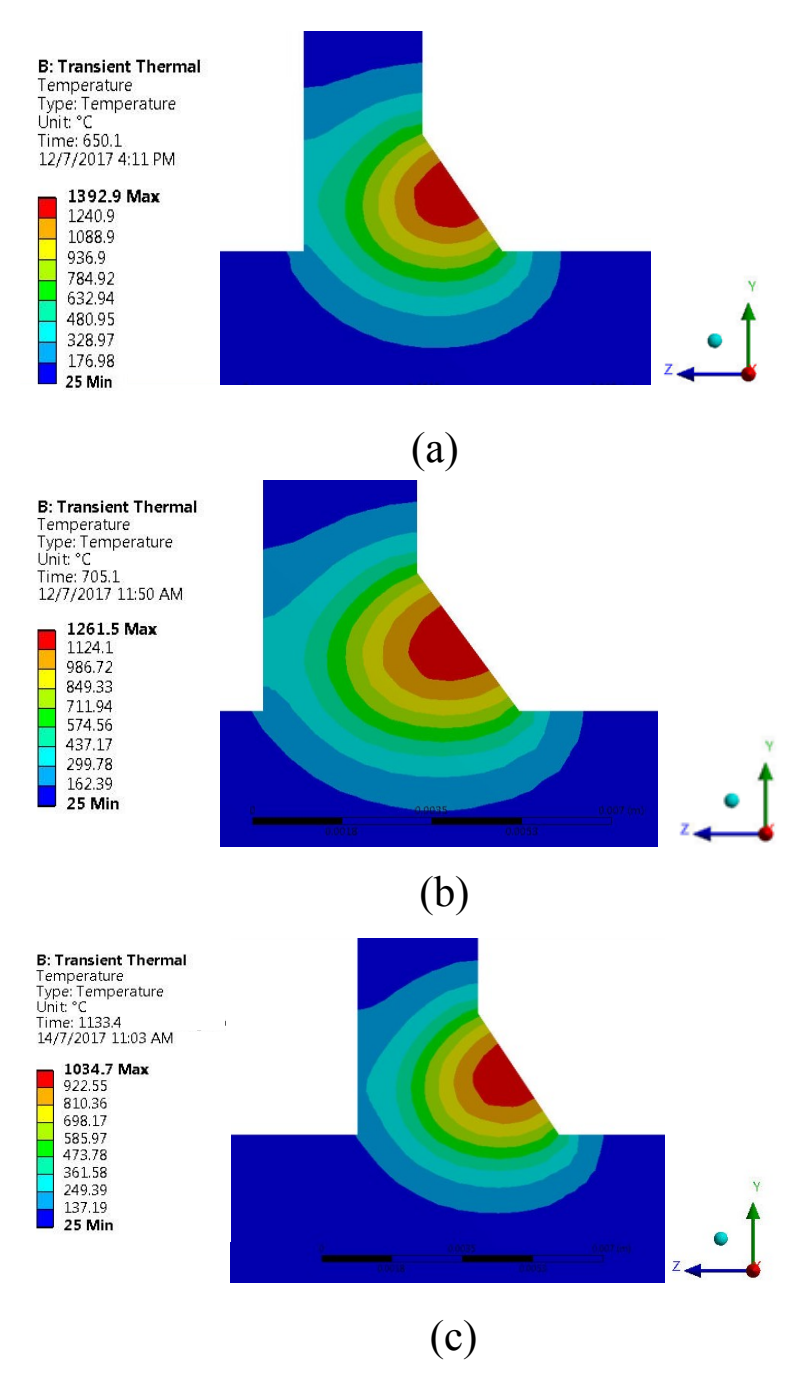


Fig. 11 Weld pool profile of laser welding at constant laser power of 4.0 kW with varying welding speed (a) low speed at 0.9 m/min (b) intermediate speed at 1.2 m/min (c) high speed at 1.5 m/min

A clear variation of result was obtained from the simulation cases, in which the depth of FZ and the size of HAZ were decreasing with the increment in welding speed. The increase in welding speed has resulted in rapid temperature decreases as the heat source applies for a shorter period of time when it moves faster. This, in turn, affects the peak temperature and thus influences the isotherm contour during the welding simulation. This argument was also supported by Equation 1, whereby the welding speed was written in the form of exponential decay. Figure 12 illustrates the effect of the welding speed variation on the penetration depth and width of HAZ of laser welding model. From the figure, a clear trend can be observed, in which the welding speed has a substantial effect on the penetration depth and the width of HAZ. Higher welding speed will eventually decrease the penetration depth and width of

HAZ. It is assumed that the cross-sectional area did not collect enough thermal energy with increasing welding velocity since a fast welding process prevents heat from staying longer in the desired location. As expected from the lumped heat capacity equation in Swifthook and Gick model, penetration depth is inversely proportional to the welding speed, focal spot size, and power [31] as follow:

$$0.483P(1-r_f) = vwh\rho C_p T_m \tag{8}$$

where w is the weld width, v is the welding speed, h is the thickness, C_p is the specific heat capacity, ρ is the density, T_m is the melting temperature, r_f is the reflectivity, and P is the absorbed power. As mentioned previously, the size of HAZ is depended on the joint configuration, the thickness of material, peak temperature, preheat conditions and the net energy input. For single-pass welding process, the width of HAZ (for thin plate) can be estimated based on modified Rosenthal's equation of the simplified 3D heat flow equation. A theoretical relationship between the cross-sectional geometry of weld bead and welding process parameters was derived by [32] where:

$$n_{ch} = \frac{Q_{rate} v}{4\pi \kappa^2 \rho C_p (T_m - T_o)} \tag{9}$$

$$D_{ch} = \frac{Y_{HAZ}v}{4\kappa} \tag{10}$$

where T_0 is the ambient temperature in Kelvin, Q_{rate} is the rate of heat input, ρ is the density, C_P is the specific heat capacity, κ is the thermal diffusivity, ν is the welding speed, Y_{HAZ} is the distance from the weld root center, D_{ch} is the dimensionless weld depth, n_{ch} is the dimensionless operating parameter, and T_m is the melting temperature in Kelvin. The relationship of D_{ch} and n_{ch} can be found in literature [32]. Careful observation of the above equation reveals that an increase in heat input rate will increase the size of HAZ. Therefore, the low overall heat input in laser welding brings less dissolved precipitates and thereby narrowed softened regions (HAZ).

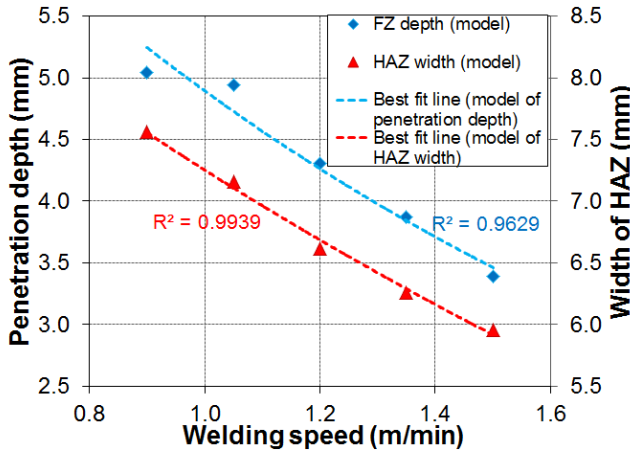


Fig. 12 Plots of penetration depth and width of HAZ against welding speed variation with constant laser power of 4.0 kW

5 Conclusion

Through the thermal analysis of laser welding, it is evident that heat input and welding speed have a significant effect on the penetration depth and size of HAZ. It was found that in most cases the model could yield an almost accurate result with the prediction error of below 10%. In all cases of simulation, the penetration depth and the width of HAZ have the tendency to increase with the increase of heat input. However, a slight decrease in the HAZ width was observed for the case of 0.3 kJ/mm heat input. On the other hand, the welding speed has a

substantial effect on the penetration depth and the width of HAZ. Higher welding speed will eventually decrease the penetration depth and width of HAZ. This effect can be seen in all simulation cases.

Acknowledgements. The authors acknowledge the support from Malaysia Ministry of Education (MoE) under MyBrain15 scheme. This research was partially funded through research grants of 1001/PMEKANIK/814235 and PJP/2018/FKP(5A)9/S01585.

References

- 1. Collette MD (2007) The impact of fusion welds on the ultimate strength of aluminium structures. In: 10th Int. Symp. Pract. Des. Ships Other Float. Struct., Houston, Texas, USA
- 2. Duricic D, Aleksic S, Scepanovic B, Lucic D (2017) Experimental, theoretical and numerical analysis of K-joint made of CHS aluminium profiles. Thin-Walled Structures 119:58–71.
- 3. Imam Fauzi ER, Jamil MSC, Samad Z, Muangjunburee P (2017) Microstructure analysis and mechanical characteristics of tungsten inert gas and metal inert gas welded AA6082-T6 tubular joint: A comparative study. Trans. Nonferrous Met. Soc. China. 27:17–24. doi:10.1016/S1003-6326(17)60003-7.
- 4. CEN (2007) Eurocode 9. Design of aluminium structures. Part1-1: General structural rules. EN-1999-1-1.
- 5. Mrówka-Nowotnik GZ, Sieniawski J (2005) Influence of heat treatment on the microstructure and mechanical properties of 6005 and 6082 aluminium alloys. J. Mater. Process. Technol. 162163:367–372. doi:10.1016/j.jmatprotec.2005.02.115.
- 6. Sánchez-Amaya JM, Delgado T, González-Rovira L, Botana FJ (2009) Laser welding of aluminium alloys 5083 and 6082 under conduction regime. Appl. Surf. Sci. 255:9512–9521. doi:10.1016/j.apsusc.2009.07.081.
- 7. Sasabe S, Matsumoto T (2010) Mechanical properties of A6082 welded joints with Nd-YAG laser. Keikinzoku Yosetsu/Journal Light Met. Weld. Constr. 48:19–27. doi:10.1080/09507116.2011.590670.
- 8. Oliveira AC, Siqueira RHM, Riva R, Lima MSF (2015) One-sided laser beam welding of autogenous T-joints for 6013-T4 aluminium alloy. Mater. Des. 65:726–736. doi:10.1016/j.matdes.2014.09.055.
- 9. Zhang C, Gao M, Zeng X (2016) Effect of microstructural characteristics on high cycle fatigue properties of laser-arc hybrid welded AA6082 aluminum alloy. J. Mater. Process. Technol. 231:479–487. doi:10.1016/j.jmatprotec.2016.01.019.
- 10. Rohde M, Markert C, Pfleging W (2010) Laser micro-welding of aluminum alloys: Experimental studies and numerical modeling. Int. J. Adv. Manuf. Technol. 50:207–215. doi:10.1007/s00170-009-2510-0.
- 11. Zain-ul-abdein M, Nélias D, Jullien JF, Boitout F, Dischert L, Noe X (2011) Finite element analysis of metallurgical phase transformations in AA 6056-T4 and their effects upon the residual stress and distortion states of a laser welded T-joint. Int. J. Press. Vessel. Pip. 88:45–56. doi:10.1016/j.ijpvp.2010.10.008.
- 12. Moarrefzadeh A (2012) Finite-element simulation of aluminum temperature field and thermal profile in laser welding process. Indian J. Sci. Technol. 5:3177–3182.
- 13. Volpp J (2012) Investigation on the influence of different laser beam intensity distributions on keyhole geometry during laser welding. Phys. Procedia. 39:17–26. doi:10.1016/j.phpro.2012.10.009.
- 14. Mazar Atabaki M, Nikodinovski M, Chenier P, Ma J, Liu W, Kovacevic R (2014) Experimental and numerical investigations of hybrid laser arc welding of aluminum

- alloys in the thick T-joint configuration. Opt. Laser Technol. 59:68–92. doi:10.1016/j.optlastec.2013.12.008.
- 15. Ma T, den Ouden G (1999) Softening behaviour of Al–Zn–Mg alloys due to welding. Mater. Sci. Eng. A. 266:198–204. doi:10.1016/S0921-5093(99)00020-9.
- 16. Hirose A, Kurosawa N, Kobayashi KF, Todaka H, Yamaoka H (1999) Quantitative evaluation of softened regions in weld heat-affected zones of 6061-T6 aluminum alloy Characterizing of the laser beam welding process. Metall. Mater. Trans. A. 30:2115–2120. doi:10.1007/s11661-999-0022-z.
- 17. Zervaki AD, Haidemenopoulos GN (2007) Computational kinetics simulation of the dissolution and coarsening in the HAZ during laser welding of 6061-T6 Al-alloy. Weld. J. 86:211–221.
- 18. Wu SC, Yu X, Zuo RZ, Zhang WH, Xie HL, Jiang JZ (2013) Porosity, element loss, and strength model on softening behavior of hybrid laser arc welded Al-Zn-Mg-Cu alloy with synchrotron radiation analysis. Weld. J. 92:62–71.
- 19. SIMTech (2017) 6 kW High Power Fiber Laser. https://www.a-star.edu.sg/simtech/Research/Equipment-Facilities-in-SIMTech/tid/52/6-kW-High-Power-Fiber-Laser.aspx. Accessed 19 January 2017.
- 20. Goldak JA, Chakravarti A, Bibby MJ (1984) A new finite element model for welding heat source. Met. Trans B. 15B:299–305.
- 21. Pavelic V, Tanbakuchi R, Uyehara OA, Mayers PS (1969) Experimental and computer temperature histories in gas tungsten arc welding of thin plates. Weld. J. 48:295–305.
- 22. Goldak JA, Akhlaghi M (2005) Computational welding mechanics. Springer Science & Business Media Inc.
- 23. Winczek J (2016) The analysis of temporary temperature field and phase transformations in one-side butt-welded steel flats. Join. Technol., InTech.
- 24. Beyer E (1995) Schweissen mit Laser (in German). Springer-Verlag.
- 25. BSI (1991) British Standard BS 8118: Part 1: 1991, London.
- 26. Jamil MSC, Fauzi ERI, Juinn CS, Sheikh MA (2015) Laser bending of pre-stressed thin-walled nickel micro-tubes. Opt. Laser Technol. 73:105–117. doi:10.1016/j.optlastec.2015.04.012.
- 27. Mikron Instrument Company (2016) Table of emissivity of various surfaces, Schaffhausen, Swiss.
- 28. Matusiak M (1999) Strength and ductility of welded structures in aluminium alloys. PhD Thesis, Norwegian University of Science and Technology.
- 29. Myhr OR, Grong Ø (1991) Process modelling applied to 6082-T6 aluminium weldments—I. Reaction kinetics. Acta Metall. Mater. 39:2693–2702. doi:10.1016/0956-7151(91)90085-F.
- 30. Ambriz RR, Jaramillo D (2014) Mechanical behavior of precipitation hardened aluminum alloys welds. In: Light Met. Alloy. Appl., InTech, pp. 35–59. doi:10.5772/58418.
- 31. Steen WM, Mazumder J (2010) Laser welding. Laser Mater. Process., Springer.
- 32. Christensen N, Davies VL, Gjermundsen K (1965) Distribution of temperatures in arc welding. Br. Weld. J. 12:54–75.